Hydrothermal Phase Transformation of Bicontinuous Cubic Mesoporous Material AMS-6

Rambabu Atluri,[†] Niklas Hedin,[‡] and Alfonso E. Garcia-Bennett*,[†]

Nanotechnology and Functional Materials, Department of Engineering Sciences, The Ångström Laboratory, Uppsala University, Box 534, SE-751 21 Uppsala, Sweden, and Materials Chemistry Research Group, Department of Physical, Inorganic and Structural Chemistry, Arrhenius Laboratory, Stockholm University, SE-106 91 Stockholm, Sweden

Received August 27, 2007. Revised Manuscript Received November 26, 2007

The controlled synthesis of ordered anionic surfactant templated mesoporous silica with cubic $Ia\bar{3}d$ structure (AMS-6) is reported via prolonged periods of hydrothermal treatment (HT). The cubic $Ia\bar{3}d$ mesophase transforms to hexagonal *p6mm* after 8 days of HT at 100 °C. Surprisingly, the hexagonal phase is stable only for a limited period after which a reversal to the cubic $Ia\bar{3}d$ mesostructure is observed. Characterization methods such as powder X-ray diffraction (XRD), electron microscopy (SEM, TEM), N_2-isotherms, magic-angle spinning (MAS) ^{29}Si NMR spectroscopy, and thermogravimetric analysis (TGA) have been employed to follow structural and textural changes of the materials prepared. Data show that the resultant mesostructure and its textural properties are highly dependent on the period of HT with less unit-cell shrinkage on calcination after extensive HT. Furthermore, evidence of two different solid−solid phase mechanisms during HT is presented. The initial transition is consistent with a restructuring of the surfactant packing and a depletion of the organic moieties from the organo-silica wall as evident from ^{29}Si NMR spectroscopy. The return to the bicontinuous cubic phase is driven by changes in charge matching at the organic−inorganic interface as a result of increases in the polymerization of the silica wall. The textural properties, and in particular the presence or absence of surface porosity, has been controlled through variations in hydrothermal treatment. These are associated with specific growth directions of cubic AMS-6 crystals. The synthetic method described allows us to easily prepare phase pure and intermediate mesostructured nanoparticles.

Introduction

Even though mesoporous materials with long-range order have been studied for more than 15 years,[1,2] the number of potential applications is still increasing. This is because the long-range order in these materials exist in a wide number of well-defined two- and three-dimensional (3D) structures including tetragonal, cubic, hexagonal, or lamellar structures.[3] Another reason for the large potential of these mesoporous materials is that their preparation relies on the use of soft templates allowing an accurate control of the pore sizes in the hard silica matrix. Many research studies have been devoted to developing high-quality mesoporous materials and this has resulted in a series of mesoporous families such as the M41S,[4] FSM-*n*,[5] HMS-*n*,[6] SBA-*n*,[7,8] FDU-*n*,[9,10] and MSU-*n*.[11] More recently, applied work is being devoted to use high-surface-area mesoporous particles, monoliths, and thin films in a variety of applications including as catalysts and catalyst−supports; sensors, in diagnostic tools; as adsorbents, in chromatography; and as drug-delivery vehicles.[12]

A range of synthesis mechanisms based on liquid crystal/supramolecular templating, cooperative self-assembly, neutral templating, and evaporation-induced self-assembly have been proposed for the synthesis of mesoporous materials.[13] Mesostructures can be templated using various surfactants (e.g., cationic, anionic, neutral, triblock copolymers). It is clear that there is no one single mechanism that fits all synthesis methods and that the preparation of mesoporous materials is versatile with respect to synthesis conditions. Rearrangement of the surfactant/silica composite, i.e., phase

* Corresponding author. E-mail: alfonso.garcia@angstrom.uu.se.
[†] Uppsala University.
[‡] Stockholm University.

(1) Kresge, C. T.; Leonowicz, M. E.; Roth, W. J.; Vartuli, J. C.; Beck, J. S. *Nature* **1992**, *359*, 710.
(2) Yanagisawa, T.; Shimizu, T.; Kuroda, K.; Kato, C. *Bull. Chem. Soc. Jpn.* **1990**, *63*, 988.
(3) Terasaki, O.; Ohsuna, T.; Liu, Z.; Sakamoto, Y.; Garcia-Bennett, A. E. *Stud. Surf. Sci. Catal.* **2004**, *148*.
(4) Beck, J. S.; Vartuli, J. C.; Roth, W. J.; Leonowicz, M. E; Kresge, C. T.; Schmitt, K. D; Chu, C. T. W.; Olson, D. H.; Sheppard, E. W.; McCullen, S. B.; Higgins, J. B.; Schlenker, J. L. *J. Am. Chem. Soc.* **1992**, *114*, 10834.
(5) Inagaki, S.; Fukushima, Y.; Kuroda, K. *Chem. Commun.* **1993**, *680*.
(6) Tanev, P. T.; Pinnavaia, T. J. *Science* **1995**, *267*, 865.
(7) Huo, Q. S.; Leon, R.; Petroff, P. M.; Stucky, G. D. *Science* **1995**, *268*, 1324.
(8) Zhao, D. Y.; Huo, Q. S.; Feng, J. L.; Chmelka, B. F.; Stucky, G. D. *J. Am. Chem. Soc.* **1998**, *120*, 6024.
(9) Liu, X. Y.; Tian, B. Z.; Yu, C. Z.; Gao, F.; Xie, S. H.; Tu, B.; Che, R. C.; Peng, L.-M.; Zhao, D. *Angew. Chem., Int. Ed.* **2002**, *41*, 3876.
(10) Yu, T.; Zhang, H.; Yan, X. W.; Chen, Z. X.; Zou, X. D.; Oleynikov, P.; Zhao, D. Y. *J. Phys. Chem. B* **2006**, *110*, 21467.
(11) Bagshaw, S. A.; Prouzet, E.; Pinnavaia, T. J. *Science* **1995**, *269*, 1242.
(12) Taguchi, A.; Schüth, F. *Microporous Mesoporous Mater.* **2005**, *77*, 1.
(13) Wan, Y.; Zhao, D. Y. *Chem. Rev.* **2007**, *107*, 2821.

10.1021/cm702440n CCC: $40.75 © 2008 American Chemical Society
Published on Web 05/20/2008

transformations during the synthesis, have been observed in all mechanism proposed. Phase transformations from lower interfacial curvature to stable higher curvature structures as exemplified by the transition from cubic 3D cylindrical MCM-48 to hexagonal 2D cylindrical pore MCM-41 are common in the synthesis literature.[14,15] On the other hand, new mesostructures can be obtained through changes in the micellar conformation by inducing surfactant mesophases to undergo controlled phase transitions. Varying silica sources (e.g., TEOS, TMOS, TPOS),[16] additions of cosolvents,[8,17] and introducing ionic species to the synthesis medium,[18,19] are typical methods to induce phase transformations.

The formation of "phase-pure" mesoporous structures strongly depends on synthesis conditions such as temperature, synthesis time, pH, solvents, silica/surfactant ratios, and drying/calcination routes.[20–22] The synthesis pH conditions strongly determines the rate of silica hydrolysis and condensation, whereas hydrothermal treatment strongly affects the silica polymerization and ultimately improves the structural properties. At lower pH conditions, the number of fully condensed silicon atoms increases with temperature showing changing condensation rates of silica (i.e., $(Si-O-Si)_n$). This is reflected in an increasing Q^4/Q^3 ratio as determined from ^{29}Si NMR spectra (where Q^n: $Si(OSi)_n(OH)_{4-n}$). Typically, hydrothermal treatment (HT) is conducted at temperatures of about 100 °C for mesoporous materials synthesized under acid conditions.

Different mechanisms have been proposed for the mesophase transformations appearing under HT. These include solid-state phase transitions;[21] dissolution and reprecipitations;[23] epitaxial phase transitions;[16,24] and layer by layer models of crystal growth.[25] Understanding the thermal and kinetic behavior of phase transformations and their mechanisms is important to reach novel structural and textural properties as well as in scale-up processes in industrial preparations.

In this work, we have studied the HT-induced transformations in anionic surfactant-templated mesoporous silica (AMS-*n*) materials.[26] The AMS silicas are a relatively new family of materials that have attracted significant attention because of their large number of well-defined structures.[27,28] Using a variety of co-structure-directing agents (CSDA), one can introduce quaternized aminopropylsiloxane (e.g., 3-aminopropyltriethoxysilane, APES) as a co-condensing silica source that strongly interacts with the anionic headgroup and is covalently bonded to the inorganic silica wall. This could very well have a significant entropic contribution with increased matching of charge density by which the assembly process proceeds.[29] Additionally, this method allows for a direct incorporation of functional groups within the porous surface after the removal of surfactants by solvent extraction methods.[30,31] The AMS-*n* synthesis route has been shown to be extremely sensitive to synthesis parameters leading to a variety of structural changes. It has been demonstrated by Che and associates that the degree of ionization of the anionic surfactant headgroup greatly affects the structural properties of AMS-*n* products.[32] Recently, we have in a further publication showed that the AMS-*n* structures can be controlled by adjusting the addition of CSDA and TEOS.[33]

Here, we present a systematic study of the hydrothermal treatment (HT)-induced phase transitions in a certain AMS solid, with well-defined bicontinuous cubic mesoporous structure. This structure has been previously termed AMS-6 (spacegroup $Ia\bar{3}d$). We report the effect of HT over long time periods (up to 60 days). A combination of XRD, SEM, TEM and N_2 sorption isotherm data allows us to study the evolution of both structural and textural properties for the AMS solids prepared at varying HT times. Data reveal that two phase transitions occur consequently, one from $Ia\bar{3}d$ to *p6mm* and another from *p6mm* back to $Ia\bar{3}d$. Via the synthesis protocol presented here, we isolated intermediate phases between the "*p6mm* back to $Ia\bar{3}d$" transition. This second transition showed slower kinetics than the first transformation. The phase-transformation behavior is rationalized on the basis of data from TGA and MAS ^{29}Si NMR spectroscopy, allowing a transition mechanism to be proposed.

Materials and Methods

For the synthesis of AMS-6, *N*-Lauroyl-*L*-Alanine (C_{12}Ala, Nanologica AB, Sweden) is used as surfactant, 3-aminopropyl triethoxysilane (APES, Aldrich) as CSDA and tetraethyl orthosilicate (TEOS, Aldrich) as silica source. All chemicals were used as received. The general procedure for the synthesis of AMS-6 materials has already been reported.[26–33] The revised synthesis procedure employed in this work is shown schematically in Figure 1. In a typical synthesis, a homogeneous solution of C_{12}Ala (0.10 g) in distilled water (20 g) is kept at 80 °C for 24 h under static conditions. The surfactant solution was stirred for 10 minuets before APES (0.10 g) addition and TEOS (0.51 g) was added 3 min after APES addition. The solution was stirred for another 15 min at 80

(14) Diaz, I.; Perez-Pariente, J.; Terasaki, O. *J. Mater. Chem.* **2004**, *14*, 48.
(15) Flodstrom, K.; Wennerstrom, H.; Teixeira, C. V.; Amenitsch, H.; Linden, M.; Alfredsson, V. *Langmuir* **2004**, *20*, 10311.
(16) Landry, C. C.; Tolbert, S. H.; Gallis, K. W.; Monnier, A.; Stucky, G. D.; Norby, F.; Hanson, J. C. *Chem. Mater.* **2001**, *13*, 1600.
(17) Anderson, M. T.; Martin, J. E.; Odinek, J. G.; Newcomer, P. P. *Chem. Mater.* **1998**, *10*, 311.
(18) Flodstrom, K.; Alfredsson, V.; Kallrot, N. *J. Am. Chem. Soc.* **2003**, *125*, 4402.
(19) Naik, S. P.; Fan, W.; Ogura, M.; Okubo, T. *J. Porous Mater.* **2006**, *13*, 303.
(20) Gross, A. F.; Le, V. H.; Kirsch, B. L.; Riley, A. E.; Tolbert, S. H. *Chem. Mater.* **2001**, *13*, 3571.
(21) Gross, A. F.; Yang, S.; Navrotsky, A.; Tolbert, S. H. *J. Phys. Chem. B* **2003**, *107*, 2709.
(22) Tolbert, S. H.; Landry, C. C.; Stucky, G. D.; Chmelka, B. F.; Norby, P.; Hanson, J. C.; Monnier, A. *Chem. Mater.* **2001**, *13*, 2247.
(23) Petitto, C.; Galarneau, A.; Driole, M-F.; Chiche, B.; Alonso, B.; Di Renzo, F.; Fajula, F. *Chem. Mater.* **2001**, *17*, 2120.
(24) Kamiya, S.; Tanaka, H.; Che, S.; Tatsumi, T.; Terasaki, O. *Solid State Sci.* **2003**, *5*, 197.
(25) Yang, H.; Coombs, N.; Ozin, G. A. *Nature* **1997**, *386*, 692.
(26) Che, S.; Garcia-Bennett, A. E.; Yokoi, T.; Sakamoto, K.; Kunieda, H.; Terasaki, O.; Tatsumi, T. *Nat. Mater.* **2003**, *2*, 801.
(27) Garcia-Bennett, A. E.; Terasaki, O.; Che, S.; Tatsumi, T. *Chem. Mater.* **2004**, *16*, 813.
(28) Garcia-Bennett, A. E.; Kupferschmidt, N.; Sakamoto, Y.; Che, S.; Terasaki, O. *Angew. Chem., Int. Ed.* **2005**, *44*, 5317.
(29) Michael, A. S. *Ind. Eng. Chem.* **1965**, *57*, 32.
(30) Yokoi, T.; Yoshitake, H.; Tatsumi, T. *Chem. Mater.* **2003**, *15*, 4536.
(31) Han, L.; Ruan, J.; Li, Y.; Terasaki, O.; Che, S. *Chem. Mater.* **2007**, *19*, 2860.
(32) Gao, C.; Qiu, H.; Zeng, W.; Sakamoto, Y.; Terasaki, O.; Sakamoto, K.; Chen, Q.; Che, S. *Chem. Mater.* **2006**, *18*, 3904.
(33) Garcia-Bennett, A. E.; Brohede, U.; Hedin, N.; Hodgkins, R. P.; Strømme, M. *Langmuir* **2007**, *23*, 9875.

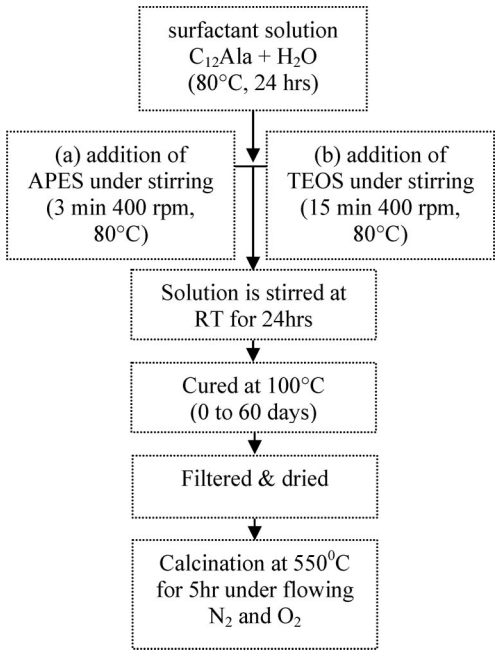

Figure 1. Schematic procedure for the synthesis of AMS-6(x) materials.

°C in a closed bottle. The synthesis gel was subsequently stored at room temperature (RT) under stirring for 24 h. The final synthesis mixture was kept sealed and without stirring at 100 °C for periods between 0 and 60 days. The solid product was filtered and dried at RT and under atmospheric pressure conditions. The molar composition of the reaction mixtures was C_{12}Ala:APES:TEOS:H_2O 1:1.25:6.7:309.1. The solids are denoted AMS-6(x), where x is the length of hydrothermal treatment (HT) in days. To ensure that the phase transformations were not due to water loss from the synthesis vessels, samples were prepared in stainless steel Teflon lined autoclaves (150 mL, Parr). Results obtained from these samples confirmed the synthesis of a hexagonal phase at 10 days and the cubic phase after 20 days.

Low-angle X-ray powder diffraction (XRD) patterns were performed on an X'Pert Pro diffractometer using Cu Kα radiation ($\lambda = 1.5418$ Å) at 45 kV and 40 mA. The diffraction patterns were recorded between 1 and 6° 2θ using an increment of 0.04° 2θ and a 60 s step time.

TEM was conducted with a JEOL-3010 microscope, operating at 300 kV (Cs 0.6 mm, resolution 1.7 Å). Images were recorded using a CCD camera (model Keen View, SIS analysis, size 1024 × 1024, pixel size 23.5 × 23.5 μm) at 30 000−100 000× magnification using low-dose conditions on as-synthesized and calcined samples. Scanning electron microscopy (SEM) images were obtained using LEO 1550 operated at 2−3kV with no gold coating.

Direct polarization ^{29}Si NMR experiments were carried out on a Chemagnetics Infinity 400 spectrometer equipped with a 9.4 T wide-bore magnet operating at 79.50 MHz. A magic angle spinning (MAS) rate of 8.5 kHz was applied and a double resonance 6 mm probe head was used. The ^{29}Si NMR chemical shift scale was externally calibrated with the tetrakis(trimethylsilyl)silane (TKS, −9.8 ppm) compound and the integral intensities were estimated using the Spinsight software. Special care was taken not to saturate the ^{29}Si magnetization. A recycling delay of 1400 s, more than 5T1, was used to avoid spectral distortion from uneven saturation patterns. A ∼70° pulse was used (4.8 μs) and 180 transients were added for each sample in a blocked manner. A continuous ^{1}H decoupling was applied during acquisition (44 kHz).

Nitrogen adsorption/desorption isotherms were measured at liquid nitrogen temperature (−196 °C) using a Micromeritics ASAP2020 volumetric adsorption analyzer. Before the measurements the calcined silica samples were outgassed under vacuum for 10 h at 120 °C. The BET (Brunauer−Emmett−Teller) equation was used to calculate the surface area (S_{BET}) from adsorption data obtained in the relative pressure (p/p^0) range of 0.05 and 0.3. The total pore volume (V_{tot}) was calculated from the amount of gas adsorbed at $p/p^0 = 0.91$. Pore size distribution curves were derived using the density functional theory (DFT) method assuming a cylindrical pore model. The microporosities were derived from the adsorption data using t-plot analysis with thicknesses 3.5−5.0 Å via the Broekhoff−De Boer thickness equation.

Thermogravimetric analyses (TGA) were performed on Mettler TGA instrument. The as-synthesized samples were heated from 25 to 900 °C at a heating rate of 1 °C/min on an alumina holder under the flow of air at 20 mL/min.

Results and Discussions

For ease of analysis and presentation, results are presented into two sections. In the first section, the phase transformation of the AMS-6(x) samples treated from 0 to 12 days is described. In the second section, the phase transformation from 12 to 60 days of hydrothermally treated samples are further investigated.

Cubic to Hexagonal Transformation from 0 to 12 Days of HT. X-ray diffraction (XRD) patterns of calcined mesostructures prepared with hydrothermal treatment (HT) for 0−12 days are shown in Figure 2. The same synthesis conditions were used and the samples are denoted AMS-6(x), where x is the duration of the HT treatment in days. Sample AMS-6(0) shows a range of well-resolved peaks with peak positions consistent with the cubic $Ia\bar{3}d$ structure with unit-cell parameter $a_0 = 105.8$ Å. Reflections from samples AMS-6(2), AMS-6(3), and AMS-6(5) typically show more intense diffractograms, which can also be indexed by a cubic unit cell, showing an increase in the degree of order with the HT. Table 1 summarizes the structural data derived from XRD for these and similar samples obtained. The overall structures do not change during these initial 5 days, they are only getting more well defined.

Samples AMS-6(8), AMS-6(9), AMS-6(10), and AMS-6(11) possess three XRD reflections corresponding to a 2D hexagonal mesostructure ($p6mm$) with an average unit cell of 51.1 Å. Sample AMS-6(12) showed broad peak positions and it is not possible to obtain structural information from XRD alone. The percentage (%) shrinkage (Table 1), as determined from XRD patterns of as synthesized and calcined samples by subtracting $((a_{\text{as-synthesized}} - a_{\text{calcined}})/a_{\text{as-synthesized}} \times 100)$, is 10.4% for AMS-6(0) and reaches a minimum of ∼0.5% with 9 days of HT. This indicates a high degree of silica polymerization with HT. After 8 days, the AMS material has undergone a transient phase transition to a 2D hexagonal structure and this order disappears after approximately 12 days.

TEM evidence confirms the formation of well ordered bicontinuous 3D cubic structures of AMS-6 (Figure 3) in samples treated for up to 5 days as well as the presence of a 2D hexagonal (p6mm) mesostructure after 8 days of HT. TEM observations reveal an external porous layer surround-

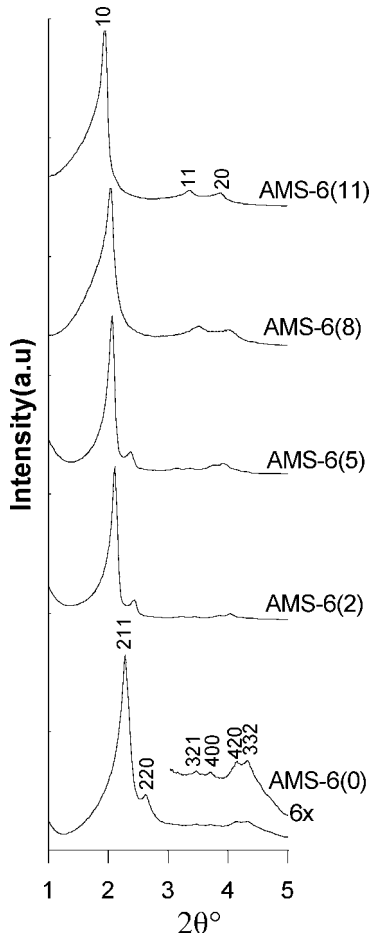

Figure 2. XRD powder diffractions of calcined samples of AMS-6(x), x = 0, 2, 8, 9, and 11 days of hydrothermal treatment. It is clear from this data that a phase transformation from a cubic to a hexagonal mesophase occurs between 5 and 8 days.

ing the mesoporous nanoparticles (Figure 3c). This layer varies in thickness from one sample to another, ranging from 5 to 20 nm, and it is surprisingly absent in AMS-6(12), which in turn showed a disordered mesostructure.

SEM images of calcined AMS-6(x) samples (see the Supporting Information) treated hydrothermally for 0−12 days show traces of elongated particles previously confirmed to be consistent with cubic AMS-6.[34] The presence of larger amounts of rod-shaped particles and traces of a chiral morphology in samples AMS-6(9) and AMS-6(11) consistent, by TEM and XRD investigations, with a hexagonal unit cell.

In this section, it is possible to conclude that a structural transformation from cubic $Ia\bar{3}d$ to hexagonal ($p6mm$) is observed through prolonged HT. The transition occurs between 5−8 days and is accompanied by a considerable decrease in unit-cell shrinkage on calcination. The transient appearance of hexagonal phase starts to end after 12 days.

Hexagonal to Cubic Transformation between 15 and 60 Days of HT. Experiments were continued to check for further structural alterations with extended HT. The XRD pattern of calcined samples AMS-6(15) show 4 peaks between 2θ values of 2−4° (Figure 4) consistent with a 2D hexagonal structure ($p6mm$) although with broader peaks than the samples treated 8−11 days. An increase in the XRD peak intensities is observed in sample AMS-6(19) between 2θ angles of 2−2.3°. It is not possible to index these peaks based on either cubic or hexagonal structures for this structure. Prolonging the HT for more than 19 days, as shown in Figure 4, results in five or more well defined diffraction peaks, with reciprocal spacing ($1/d_{hkl}$) ratios of $\sqrt{6}$, $\sqrt{8}$, $\sqrt{14}$, $\sqrt{16}$, $\sqrt{22}$ and $\sqrt{26}$, confirming the presence of cubic AMS-6 ($Ia\bar{3}d$) structure. Data indicates that the 2D hexagonal structure undergoes an isothermal phase transition to the cubic structure between 15 and 22 days of HT. It is useful to point out that, the 10 peak position of the 2D hexagonal structure becomes the 211 reflection of the cubic structure. This is consistent with previously published literature that has shown the epitaxial growth of the cubic phase from the hexagonal phase to occur via changes in silica density (modulation waves) along the 2D hexagonal (10) planes, which become the 3D cubic (211) planes.[24,35] The cell parameters of the samples AMS-6(15) and AMS-6(19) are calculated by considering (211) reflections of cubic structure respectively and are listed in Table 1. Cubic AMS-6 samples prepared at longer HT times have similar unit cell parameters as those prepared at shorter HT intervals. Sample AMS-6(60) shows the largest unit cell parameter of all cubic samples prepared here, where a_{cal} = 114.4 Å. The shrinkage with calcination increases slightly during the transition from hexagonal to cubic, where AMS-6(22) shows 4.2% shrinkage but decreases to 0.9% after 60 days of HT.

TEM images recorded on calcined samples of AMS-6(x) treated hydrothermally between 19−60 days are shown in Figure 5. All samples show a high degree of order. TEM images of AMS-6(15) (not shown) show contrast patterns and FFT diffractograms consistent with hexagonal mesostructures. The formation of an external porosity is also observed for samples AMS-6(22) and AMS-6(60), but surprisingly, no external porosity is observed at HT times of 19 and 30 days. Sample AMS-(19) shows spheroid particles with neck formations of approximately 100 nm, as shown in Figure 6a. Further TEM analysis based on tilting experiments and FFT diffractograms recorded over thin specimen regions reveal this mesostructure to be consistent with the $Ia\bar{3}d$ spacegroup symmetry, satisfying extinction conditions such as the absence of the 110 reflections along the [111] incidence (Figure 6b, inset). The TEM derived unit cell parameter, a_{TEM} = 94.8 Å, is however, considerably different from that obtained by XRD using a cubic unit cell (a_{XRD} = 109.1 Å). It is interesting to note the weak intensity of the {022} reflections from the FFT diffractogram (inset Figure 6b), in contrast with those of the {211}. Density modulations along these reflections are thought to occur during the transition from $p6mm$ to $Ia\bar{3}d$ mesophases.[24] The repeat distance between the (10) planes in the hexagonal phase observed in AMS-6(9) is 43.7 Å, whereas that observed for the (211) planes in AMS-6(19) is 38.1 Å. The $(10)_{hex}$ and $(211)_{cub}$ are the planes of highest density and the

(34) Lund, K.; Garcia-Bennett, A. E.; Terasaki, O. *J. Mater. Chem.* **2007**, *17*, 3622.

(35) Che, S.; Kamiya, S.; Terasaki, O.; Tatsumi, T. *J. Am. Chem. Soc.* **2001**, *123*, 12089.

Table 1. Textural and Structural Properties of Mesoporous Silica AMS-6(*x*), Hydrothermally Treated from 0−60 Days

sample	lattice parameter, *a* (Å)[a]	% shrinkage[b]	mesophase	DFT pore width, *D* (Å)	pore volume (cm^3/g)	surface area (m^2/g)
AMS-6(0)	105.8	10.4	$Ia\bar{3}d$	36.6	0.93	881.3
AMS-6(2)	110.8	7.8	$Ia\bar{3}d$	39.5	0.75	781.3
AMS-6(3)	109.7	8.3	$Ia\bar{3}d$	49.0	0.63	661.7
AMS-6(5)	109.6	4.4	$Ia\bar{3}d$	43.1	0.76	712.7
AMS-6(8)	39.7	1.7	*p6mm*	45.2	0.77	702.7
AMS-6(9)	51.4	0.5	*p6mm*	45.2	0.99	902.9
AMS-6(10)	51.3	1.1	*p6mm*	45.2	0.77	676.2
AMS-6(11)	52.3	1.8	*p6mm*	45.2	0.73	675.6
AMS-6(12)				42.4	0.57	479.0
AMS-6(15)	51	1.7	*p6mm*	45.2	0.81	719.4
AMS-6(19)	109.1	0.8	$Ia\bar{3}d$	45.2	0.64	587.9
AMS-6(22)	106.7	4.2	$Ia\bar{3}d$	42.4	0.61	583.9
AMS-6(30)	104	3.3	$Ia\bar{3}d$	45.2	0.62	531.5
AMS-6(60)	114.4	0.9	$Ia\bar{3}d$	45.2	0.57	536.4

[a] Calculated from calcined samples. [b] Calculated based on the XRD patterns of as-made and calcined data.

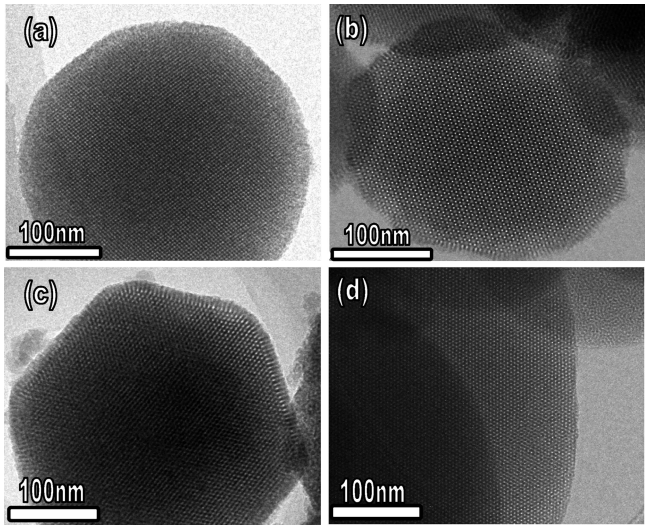

Figure 3. TEM images of AMS-6(*x*) mesoporous materials synthesized under HT for a duration of (a) 0, (b) 2, (c) 9, and (d) 12 days. An layer of surface pores can be seen in all samples prepared except that after 12 days, which shows no such surface features. It was not possible to index Fourier transform diffractograms taken from images recorded on sample AMS-6(12) using either hexagonal or cubic unit cells, and contrast patterns reveal disordered regions.

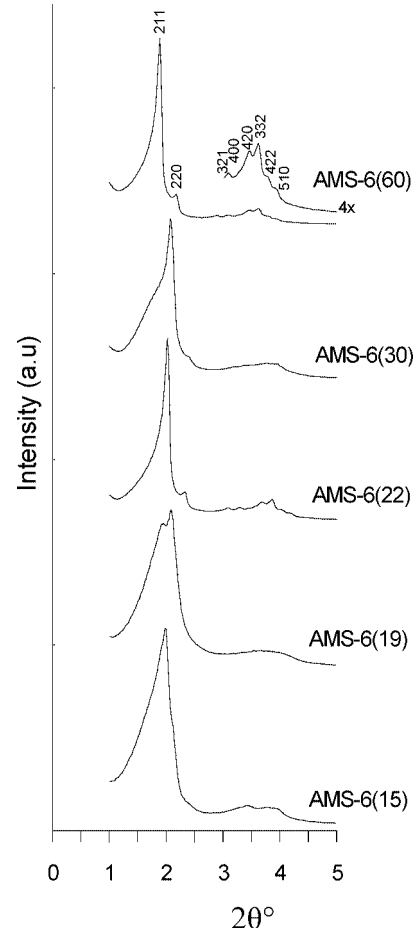

Figure 4. Powder XRD patterns of calcined mesoporous solids of AMS-6(*x*) prepared with 15, 19, 22, 30, and 60 days of HT. A phase transformation can be observed between 15 and 22 days from 2D hexagonal to 3D cubic.

growth of the hexagonal phase is highly favored along the [111] direction of the cubic structure. A detail analysis of the epitaxial growth of the hexagonal phase from the cubic phase has been conducted for surfactant systems,[36] where it was concluded, on the basis of electron density maps, that a total of 3 hexagonal cylinders are formed per cubic unit cell, where each cylinder arises from the fusion of 4 successive rod junctions on the 3-fold axis of the [111] direction. The weak {022} diffraction spots together with the unresolved XRD pattern may be indicative of an intermediate mesophase where transformation to the $Ia\bar{3}d$ phase is not complete.

TEM images of sample AMS-6(22) show monodispersed particles (Figure 5c) of the cubic mesophase, where a distinct external porosity is clearly observed. Figure 5d shows a high-magnification image of the boundary between the ordered cubic structure and the external porosity as viewed along the [111] incidence. Pore openings to the exterior of the particle can be clearly viewed protruding from the ordered structure parallel to the $h\bar{k}0$, $0k\bar{l}$, and $\bar{h}0l$ planes along a 3-fold axis of symmetry. It is well-known[36] that the bicontinuous cubic $Ia\bar{3}d$ phase typically consists of two independent interpenetrating porous networks composed of cylindrical pores joined by trifunctional connectors. These so-called external pores can be considered as surface growth features and it is clear from this, and other images, that the particle growth occurs perpendicular to the [111] incidence. These results are also consistent with the $m\bar{3}m$ point group symmetry expected for the $Ia\bar{3}d$ structure. Similar surface growth features have been also observed in the caged

(36) Mariani, P.; Amaral, L. Q.; Satumi, L.; Delacroix, H. *J. Phys. II Fr.* **1994**, *4*, 1393.

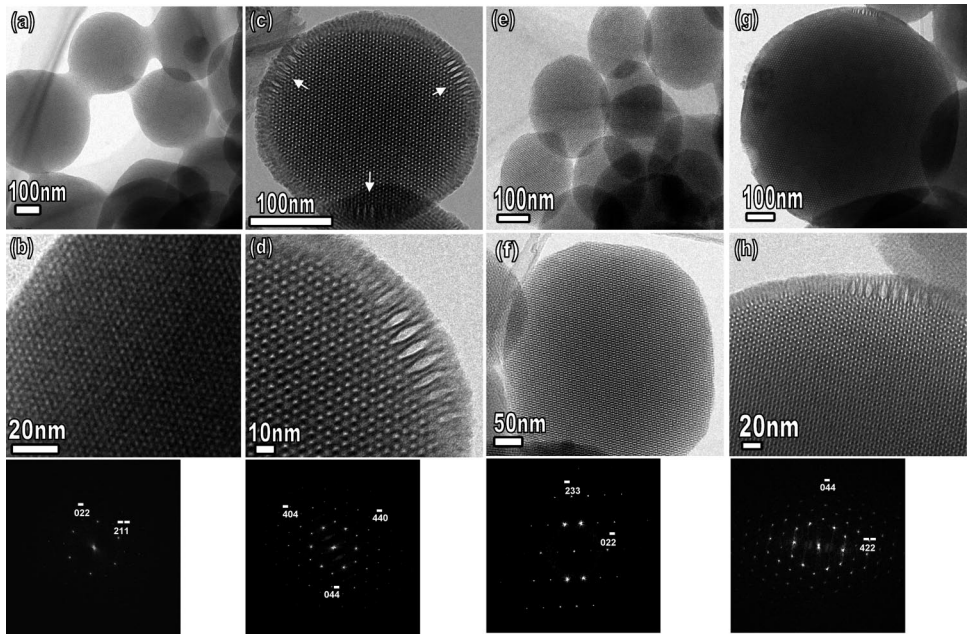

Figure 5. HRTEM of cubic samples treated for prolonged periods of HT for (a, b) 19, (c, d) 22, (e, f) 30, and (g, h) 60 days. Insets show fast Fourier transform (FFT) diffractograms recorded over thin regions of particles shown. All images are recorded along the [111] incidence, except (f), which is recorded along the [311] incidence.

structure AMS-8 ($Fd\bar{3}m$) when the particle growth kinetics was slowed down by the use of a polymeric dispersant.[37]

Calcined samples of AMS-6(30) and AMS-6(60) shows contrast patterns and FFT diffractograms consistent with the cubic structure, however the former shows the absence of external porosity and a high degree of monodispersed particles, while the latter displays surface porosity similar to that encountered in previous samples.

SEM images recorded on AMS-6(x) samples treated for longer HT intervals are shown in Supporting Information. After 22 days of HT, monodispersed particles with uniform size distribution of about 580nm were formed. In addition, no elongated particles or those showing a chiral morphology are seen after HT treatment of 22 days. There is no considerable increase in particle size with longer HT treatment.

A detailed analysis of the structural data suggests that transformation from cubic to hexagonal is kinetically faster—between 3 and 5 days of the HT treatment—than the hexagonal to cubic transformation, which shows clearly intermediate mesophases over a longer time period between 15 and 22 days of HT treatment. In the AMS system reported here, where an anionic headgroup in combination with a co-structure-directing agent is used, the electrostatic environment around the surfactant headgroup (including entropic contributions) has been found to play a leading role in the effective surfactant curvature. Several mesophase transitions involving complex restructuring of surfactant packing have been reported through addition of NaOH and HCl to the synthesis mixture.[32] Mesophase transitions from cubic $Ia\bar{3}d$ to the 2D hexagonal $p6mm$, involve an increase of the surfactant packing parameter, g, which has been previously used to quantify changes in micellar curvatures.[20,22] It is thought that when a surfactant is heated, thermally excited hydrocarbon chains increase the overall molecular micellar volume, leading to increases in g. Short HT times with high charge densities on the silica wall favor phase transformations, as is shown experimentally elsewhere. However, such curvature changes alone, do not explain the slow time scale of phase transformations observed here.

The degree of silica condensation/polymerization can be followed from ex situ ^{29}Si NMR spectra (Figure 6) of as-synthesized AMS-6(x) samples. In addition, it is possible to determine the ratio of organic-silica and inorganic silica in these AMS-6(x) samples with this technique. The spectra of AMS-6(x) samples consist of three distinct signals corresponding to Q^4, Q^3, and T^3 moieties. The Q^4 signal represents silicon atoms surrounded by four oxygen atoms, i.e., fully condensed silica moieties. The Q^3 signal represents silica moieties with a $-$OH or a $-O^-$ group attached. The T^3 moieties show the presence of the organoalkoxysilane CSDA. The ^{29}Si NMR spectra indicate AMS-6 samples prepared with short HT times have a less well-formed silica network. The initial sample AMS-6(0) has a less condensed framework observed from the higher $Q^3/(Q^4 + Q^3)$ ratios. In addition this sample has a large $T^3/(Q^4 + Q^3)$ ratio. Both these ratios decrease with the HT. We speculate that this exclusion (or decomposition) of organo-silica moieties and condensation of the silica network are the molecular reasons for the two phase transitions found. From Figure 6 it is clear that the relative amount of organo-silica moieties is reduced already after 9 days. A transition from a bicontinuous cubic structure to a hexagonal structure occurring during this period cannot

(37) Garcia-Bennett, A. E.; Lund, K.; Terasaki, O. *Angew. Chem., Int. Ed.* **2006**, *45*, 2434.
(38) Gross, A. F.; Yang, S.; Navrotsky, A.; Tolbert, S. H. *J. Phys. Chem. B* **2003**, *107*, 2709.
(39) Hecht, E.; Hoffmann, H. *Langmuir* **1994**, *10*, 86.
(40) Huo, Q.; Margolese, D. I.; Stucky, G. D. *Chem. Mater.* **1996**, *8*, 1147.

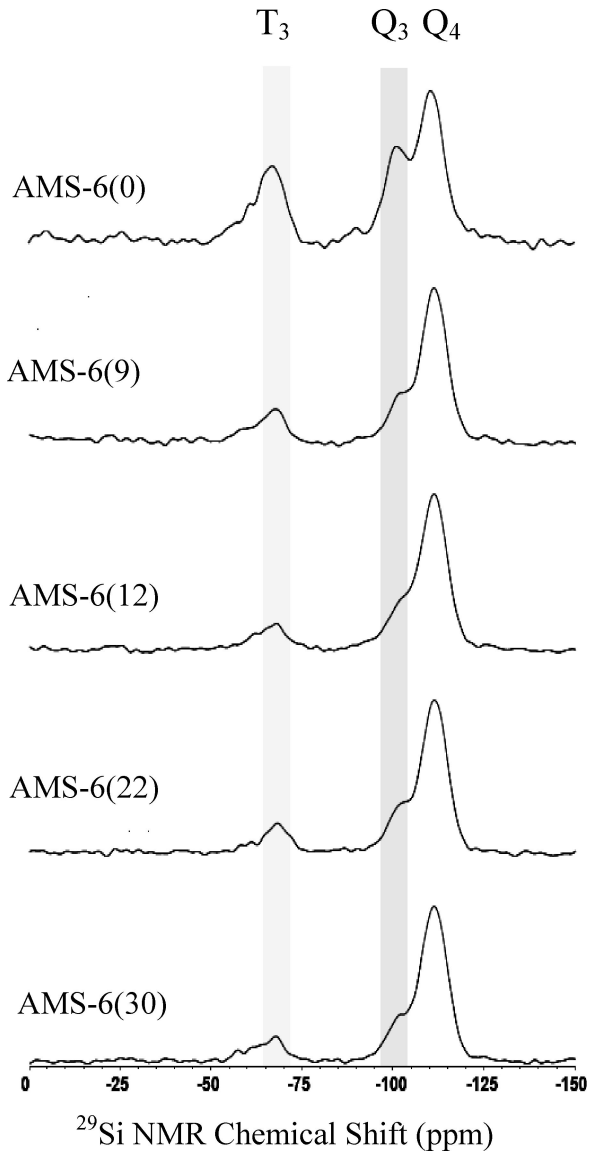

Figure 6. Magic angle spinning solid-state ^{29}Si NMR spectra of as-synthesized samples of AMS-6(*x*) mesoporous silica with 0, 9, 12, 22, and 30 days of HT.

be simply rationalized from packing reasons without an increased level of hydration or headgroup repulsion. Such repulsion or hydration can definitely be associated with the exclusion of the organo-silica and the associated changes of the properties of the inorganic wall.

The second transition from hexagonal to cubic symmetry, is consistent with the findings by Landry and associates,[16] in a study of HT induced transition from MCM-41 to MCM-48. This transition is thought to be driven by further condensation of the inorganic silica during HT. Such condensation is evident from Figure 6 via the decreasing $Q^3/(Q^4 + Q^3)$ ratio. During prolonged hydrothermal treatment, silanol groups and deprotonated silanol groups condense liberating hydroxide anions which, we argue here, increase headgroup repulsion. This leads to a change in micellar conformation as the packing of surfactant molecules tries to maintain van der Waals interactions between the hydrocarbon tails while the distance between headgroup charges increases. Navrotsky, Tolbert et al. have found through in situ calorimetric studies that reduction in the silica charge density as a result of condensation of the silica wall favors transformations to the cubic phase on energetic grounds, whereas heat treatments at high temperatures, or for prolonged times, lowers the activation barriers for transformations to occur.[38]

Further evidence of the structural differences between materials prepared here is provided by nitrogen sorption isotherms and thermal gravimetric analysis (TGA). Figure 7a shows sorption isotherms of samples that are assigned as cubic, and the Figure 7b shows samples that are characterized as hexagonal mesoporous structures. Their corresponding pore size distributions are shown in panels c and d in Figure 7, respectively. The comparative structural and textural properties of AMS-6(*x*) samples are summarized in Table 1. All the samples showed type IV nitrogen sorption isotherm. No significant hysteresis loop is observed in the desorption branch of the isotherm curve ($P/P_0 = 0.25-0.45$) owing to the small size of the pores, however for cubic samples where surface porosity is observed through TEM a hysterisis loop between $P/P_0 = 0.45-1$ is observed (AMS-6(22) and AMS-6(60) in Figure 7) indicative of a geometric constraint to the desorption process within pores larger in value than those reflected in the pore size distribution curves. A sharp increase in the volume adsorbed between the relative pressures $P/P_0 = 0.25-0.5$ reflects the narrow mesopore size distribution. As illustrated in Figure 7a, the capillary condensation step shifts in direction of larger relative pressures from 0.25 to 0.5 with the HT, indicating the increasing pore size (Figure 7c) for cubic $Ia\bar{3}d$ samples. However, samples (Figure 7b) which are assigned as hexagonal (AMS-6(8)-AMS-6(15)) show no shift in the relative pressure of the capillary condensation step, indicating a stable pore size distribution with increased HT (Figure 7d). The total mesopore volumes of materials appear to follow no trend. The highest mesopore volumes for samples prepared are obtained for; cubic sample AMS-6(0) (0.93 cm^3/g), presumably because of the poorly condensed silica wall; and for hexagonal AMS-6(9) (0.99 cm^3/g). These samples, additionally, showed the highest calculated surface areas (Table 1). Only sample AMS-6(60) showed evidence of micropores using *t*-plot analysis of the isotherm data where a small micropore area of 27.40 m^2/g and micropore volume of 0.0014 cm^3/g was calculated. The increase in pore width (Table 1 and Figure 7) on HT, combined with the rather constant lattice parameters, supports the speculation that the initial phase transformation (bicontinuous cubic to hexagonal) is driven by the exclusion of organo-silica, leaving the final material with a slightly thinner wall. Hence, the larger pore widths for the final cubic material compared with the initial AMS-6(0) solid can be explained by "etching" of the wall and a more condensed silica network.

TGA/DTG curves of the as-synthesized AMS-6(*x*) samples treated for 0, 9 and 60 days of HT are shown in Figure 8. All AMS-6(*x*) samples show three distinct stages of weight loss. The first between 120−200 °C can be accounted as decomposition of freely grafted or surface bound organoalkoxysilane groups of APES. This peak is seen to

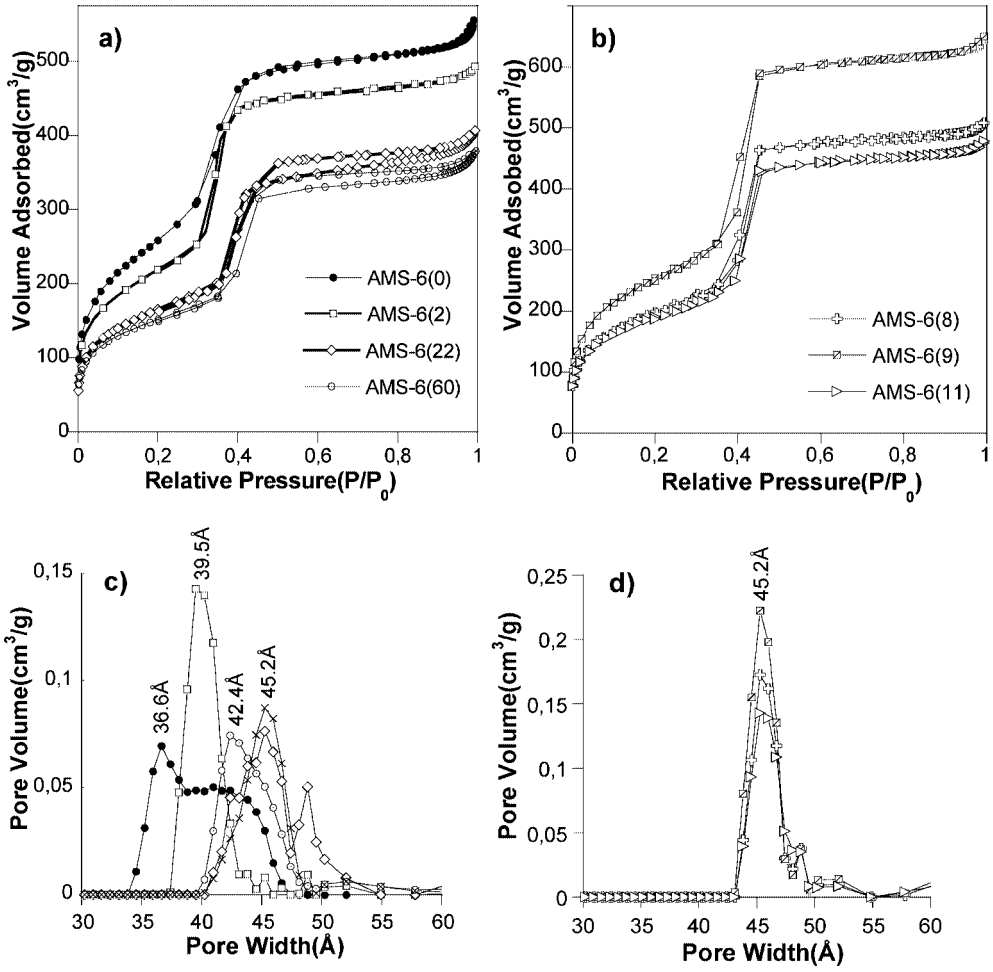

Figure 7. N_2 sorption isotherms of AMS-6(x) samples with (a) cubic ($Ia\bar{3}d$) mesostructure, (b) hexagonal structure ($p6mm$), as confirmed by XRD and TEM data. Corresponding pore size distribution curves derived using DFT and assuming a cylindrical pore geometry of (c) cubic and (d) hexagonal samples are shown below.

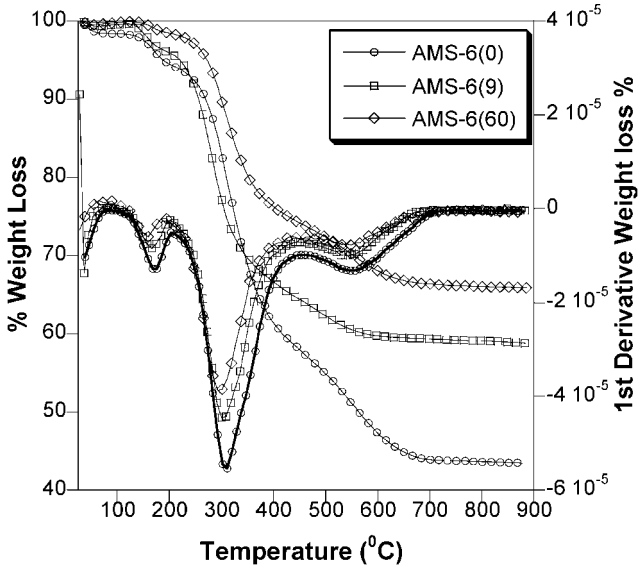

Figure 8. Thermogravimetric weight loss curves and derivative plots of as-synthesized samples of AMS-6(0), AMS-6(9), and AMS-6(60).

decrease linearly during the first 10 days of HT (Table 2) and then level of to a constant level. The leveling off is consistent with the T^3 moieties being visible in the ^{29}Si NMR spectra (Figure 6) at all investigated HT times, and that the surface organo-silica moieties are decomposed or exchanged

Table 2. Summarized Weight Losses of AMS-6(x) Samples Treated 0−60 Days of HT, Where Stage 1 Represents the Loss Due to Decomposition of Freely Grafted APES and Stage 2 the Decomposition of Reacted APES and Surfactant Molecules

sample	stage 1 (120−200 °C)	stage 2 (200−400 °C)	total loss wt %	% yield of silica
AMS-6(0)	3.9	36.8	56.6	43.4
AMS-6(2)	3.6	36.9	48.8	51.1
AMS-6(3)	3.2	28.8	39.5	60.4
AMS-6(5)	2.0	30.3	39.8	60.2
AMS-6(8)	2.2	26.3	39	61
AMS-6(9)	2.4	27.4	40.4	59.6
AMS-6(10)	2.2	25	38.2	61.8
AMS-6(11)	2.1	25.3	37.7	62.3
AMS-6(12)	1.9	22.6	35.4	64.6
AMS-6(15)	1.9	24	36.2	63.8
AMS-6(19)	2.1	24.4	37.3	62.7
AMS-6(22)	1.7	22.2	34.7	65.3
AMS-6(30)	1.6	22.2	33.7	66.3
AMS-6(60)	1.7	22.5	34	66

during the HT. These TGA data are only qualitative because it is difficult to quantify the decomposition of reacted APES (pore-wall bound) due to overlap with decomposing surfactants. TGA/DTG data obtained from solvent extracted samples (see the Supporting Information) suggets the presence of surfactant even after prolongued extraction times. The second weight loss (200−400 °C) is associated hence with the decomposition of anionic surfactant and reacted APES. These values suggest a migration of the surfactant

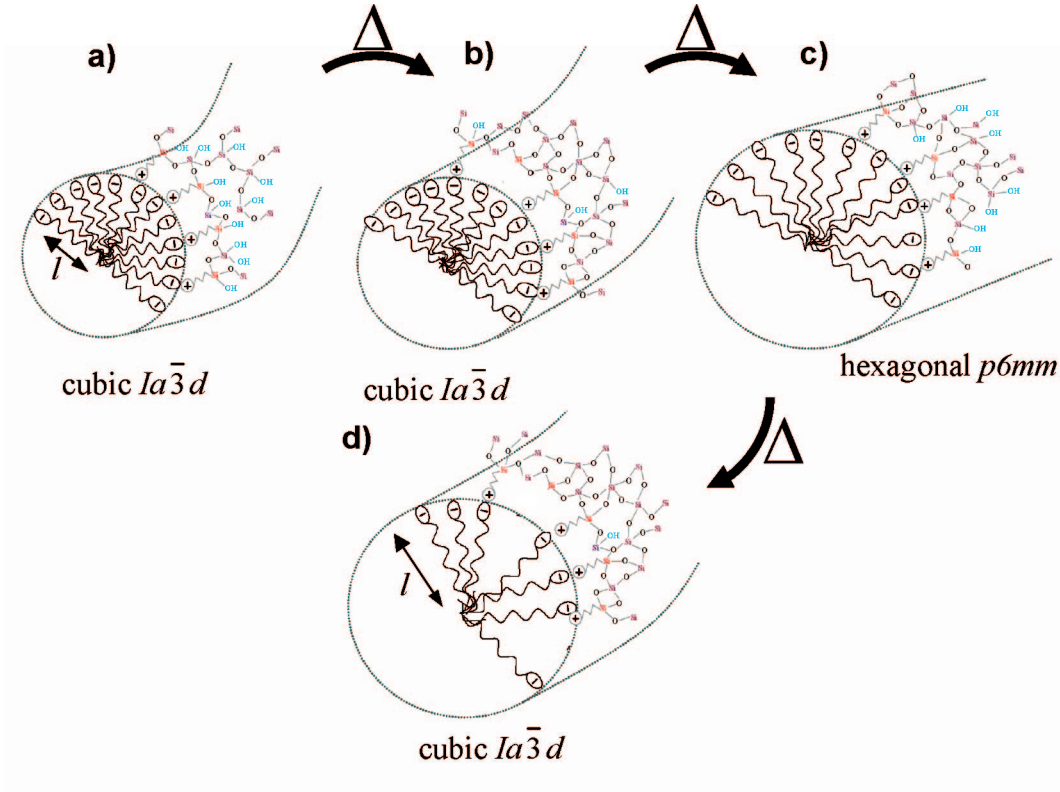

Figure 9. Schematic representation of the phase transformation in AMS-6(*x*) synthesis with HT time at the surfactant−silica interface. Silicon atoms covalently bonded to the aminopropyl group are colored red and intrawall hydroxyl groups are colored blue. The initial transformation from cubic $Ia\bar{3}d$ to hexagonal *p6mm* is governed by changes in the micellar volume as a result of thermal excitation of the hydrophobic surfactant tails and variations in the amount of CSDA at the organic−inorganic interface. Cubic phases prior to the transition have a higher pore size and a more condensed wall density than at the initial stages of HT (a, b). The transition from 3D to a 2D mesostructure is consistent with an increase in the condesation of intrawall silanol groups as observed from TGA data (c). Subsequent condensation of silanol groups together with changes in charge matching at the micellar−silica interface are thought to be responsible for the secondary transformation after prolonged (15 days) HT (d). This is also accompanied with a decrease in the surfactant/APES ratio, which may be due to degradation of the anionic surfactant.

out of the polymerizing structure with HT, perhaps due to decomposition of the surfactant via thermal degradation.[39] The third stage in the TGA/DTG curve (400−900 °C) is accompanied by condensation of silanol groups. A decrease in wt % loss due to condensation of approximately 45% is observed when the AMS-6 samples are hydrothermally treated for two (2) days, highlighting the large differences in polymerization degree and silica wall densities obtained through this short thermal treatment.

For comparison, a plot of % unit-cell shrinkage and wt % silica condensation calculated from XRD and TGA data respectively versus hydrothermal time for AMS-6(*x*) samples is shown in the Supporting Information. After 2 days HT, the silica condensation appears to closely follow the phase transformations inasmuch as there is a significant increase (30%) in silanol group condensation as a result of the mesostructure change from cubic $Ia\bar{3}d$ to *p6mm* between 5 and 8 days.

Overall, the results indicate that the phase transformation described here from cubic $Ia\bar{3}d$ to hexagonal *p6mm*, is accompanied with a higher amount of silanol group rearrangement than the reverse transformation from lower curvature to higher curvature. Data from TGA seem to confirm the initial mesophase transformation to be governed by changes in silica rearrangement through etching and increased headgroup repulsion, or hydration level, in the surfactant headgroup region of the CSDA with HT, whereas the secondary mesophase transformation is driven primarily by changes in charge matching at the silica/organic interface, because of increased polymerization of the silica wall and an increase in wall density.

A dissolution−reprecipitation mechanism under hydrothermal conditions, which has been suggested previously for hydrothermal transitions,[14,40] cannot overall be excluded for the AMS-6 system described here. Data from ^{29}Si NMR spectra shows an increase in the polymerization degree of the silicate wall with HT and no unexpected variations in the Q^4/Q^3 ratios were observed with higher HT times. An initial pH of ∼9 is attained during the synthesis which gradually reaches 6.9 after 8 days of HT and finally 7.5 after 22 days. At these pH levels, the dissolution rate is apparently still high for amorphous silica.[41] The observation of external porosity or surface features in certain samples and not others during HT must suggest an ongoing growth of the silica particles and changes in the concentration of growth "nutrients" at the growing surfaces. A certain amount of dissolution and reprecipitation must therefore occur for this to be possible, albeit at the immediate particle surface. Significant evidence of particle dissolution was observed only for AMS-6(60) samples by SEM and TEM studies, where

(41) Rimstidt, J. D.; Barnes, H. L. *Geochim. Cosmochim. Acta* **1980**, *44*, 1683.

intraparticle spaces have been observed (see the Supporting Information). It is not fully clear if the reduction of T^3 moieties is due to chemical decomposition or chemical exchange process. However, the reduction of organic moieties seems to be associated with a thinner wall and a transition from bicontinuous cubic to hexagonal form indicating, at least, that the T^3 moieties are not replaced by inorganic silica.

Conclusions

Here, we have reported the phase transformation of AMS-6 mesoporous materials via longer periods of hydrothermal treatment (HT). A schematic representation of the phase transformation presented here is shown in Figure 9. Our results suggest that the cubic ($Ia\bar{3}d$) structure is obtained only between 1−5 days and after 22 days of HT treatment. The latter is surprisingly stable as a well ordered structure is obtained even after prolonged treatment of 60 days. A 2D hexagonal mesoporous material is formed at HT between 5−22 days and intermediate samples showed little or no change in the polymerization degree as well as the high-temperature dehydration. In addition, very small changes in pore size distribution are measured for hexagonal samples, whereas cubic samples show more variations in wall density and textural properties of materials prepared with hydrothermal treatment.

Electron-microscopy-based methods show that the phase transition is due to solid−solid state mechanism. An intermediate sample between $p6mm \rightarrow Ia\bar{3}d$ has been isolated at 15 days of hydrothermal treatment, nicely corroborating previous work published on the epitaxial relationship between these two structures. TEM images shows clearly that the phase transformation proceeds along the [111] orientation of the cubic structure, where the $(10)_{hex}$ plane is commensurate with the $(211)_{cub}$ plane of the cubic phase.

The presence of external porosity has been found only in certain samples and is present in both hexagonal and cubic mesoporous materials. The formation of these surface features remains poorly understood; however, it is apparent from TEM evidence that it is closely related with the particle growth and occurs only along specific directions. In sample AMS-6(22) these have only been found along the 3-fold axis of the [111] incidence.

This hydrothermal treatment based synthesis provides a useful way to prepare high-quality structures with controllable textural properties, surface features and morphology. A lot is expected from the hydrothermal stability of mesoporous material AMS-6, which remains stable even after prolonged treatment of over 60 days of synthesis. By comparing information from ^{29}Si NMR spectroscopy and TGA, we conclude that the AMS-6 solid is initially depleted of organo-silica moieties. This depletion happens concurrently with a transition from cubic to hexagonal symmetry. At longer HT treatment times the silica network condenses and the material transform from hexagonal to cubic symmetry.

Acknowledgment. The authors express their gratitude to Prof. Andreas Fischer (Royal Institute of Technology, Sweden) for access to XRD facilities; to Professor Osamu Terasaki, Dr. Yasuhiro Sakamoto, and Dr. Kristina Lund for many helpful discussions and access to their TEM facilities of the electron microscopy center of Stockholm University. A.E.G.-B. is grateful for funding from Vetenskapsrådet (Junior Research Fellowship). N.H. thanks the Berzelii Center EXSELENT for support.

Supporting Information Available: SEM images of AMS-6(x) samples prepared with different hydrothermal times; additional TEM evidence of AMS-6(22); SEM images recorded on AMS-6(60) showing evidence of dissolution; plot of % silica shrinkage and wt % condensation of silica calculated from XRD and TGA data, respectively, versus hydrothermal time for AMS-6(x) samples prepared in this study; and TGA/DTG results of as made AMS-6 with 3days of HT and a solvent extracted sample of AMS-6(3) (PDF). This material is available free of charge via the Internet at http://pubs.acs.org.

CM702440N